Variability and origin of seismic anisotropy across eastern Canada: evidence from shear-wave splitting measurements

F.A. Darbyshire,[1] I.D. Bastow,[2] A.M. Forte,[1] T.E. Hobbs,[3] A. Calvel,[1] A. Gonzalez-Monteza,[1] and B. Schow.[4]

Corresponding author: F.A. Darbyshire, Centre de recherche GEOTOP, Université du Québec à Montréal. CP 8888 succursale Centre-Ville, Montréal, QC, H3C 3P8, Canada.
(darbyshire.fiona_ann@uqam.ca)

[1]Centre de recherche GEOTOP, Université du Québec à Montréal, Canada.

[2]Department of Earth Science and Engineering, Imperial College London, London, UK.

[3]School of Earth and Atmospheric Sciences, Georgia Institute of Technology, Atlanta, GA, USA.

[4]School of Earth Sciences, Stanford University, Stanford, CA, USA.

Abstract. Measurements of seismic anisotropy in continental regions are frequently interpreted with respect to past tectonic processes, preserved in the lithosphere as “fossil” fabrics. Models of present-day sublithospheric flow (often using absolute plate motion as a proxy) are also used to explain the observations. Discriminating between these different sources of seismic anisotropy is particularly challenging beneath shields, whose thick (≥200 km) lithospheric roots may record a protracted history of deformation and strongly influence underlying mantle flow. Eastern Canada, where the geological record spans ∼3 Ga of Earth history, is an ideal region to address this issue. We use shear-wave splitting measurements of core phases such as SKS to define upper-mantle anisotropy using the orientation of the fast-polarisation direction ϕ and delay-time δt between fast and slow shear wave arrivals. Comparison with structural trends in surface geology and aeromagnetic data helps to determine the contribution of fossil lithospheric fabrics to the anisotropy. We also assess the influence of sublithospheric mantle flow via flow directions derived from global geodynamic models. Fast-polarisation orientations are generally ENE–WSW to ESE–WNW across the region, but significant lateral variability in splitting parameters on a ≤100 km scale implies a lithospheric contribution to the results. Correlations with structural geologic and magnetic trends are not ubiquitous, however; nor are correlations with geodynamically-predicted mantle flow directions. We therefore consider that the splitting parameters likely record a combination of present-day mantle flow and older lithospheric fabrics. Consideration of both sources of anisotropy is critical in shield regions when interpreting splitting observations.

1. Introduction

Seismic anisotropy beneath the continents, in particular the ancient continental shields, provides important constraints on past and present tectonic processes, as well as the large-scale patterns of sublithospheric mantle flow. Shear-wave splitting analysis is a popular method for studying anisotropy, consisting of point-measurements at individual seismograph stations across a region of interest. The resulting splitting parameters are interpreted in the context of "fossil" fabrics preserved over long time scales in the lithosphere and/or mineral alignments reflecting mantle flow directions. Beneath the ancient cores of the continents, both factors are likely to play an important role in the depth-averaged anisotropic parameters measured.

When a shear wave encounters such an anisotropic medium, it splits into two orthogonal quasi-shear waves, one travelling faster than the other [e.g. *Silver*, 1996]. One is orientated along the fast-polarisation direction (ϕ) of the anisotropy, and the other is orientated perpendicular. The two waves travel at different speeds; hence a time lag (δt) is observed between the 'fast' and 'slow' shear waves when they arrive at the receiver. The size of the lag depends on the thickness of the anisotropic layer and/or the strength of anisotropy. The time lag between the 'fast' and 'slow' components results in non-zero energy on the tangential-component seismogram and an elliptical particle motion. The fast-polarisation orientation (ϕ) and time delay (δt) parameters provide simple measurements that characterise seismic anisotropy.

Shear wave splitting parameters can be related to present-day sublithospheric flow [e.g. *Vinnik et al.*, 1989, 1992; *Fouch et al.*, 2000; *Sleep et al.*, 2002], the preferential orientation of fluid or melt bodies [e.g. *Blackman and Kendall*, 1997], pre-existing "fossil" anisotropy frozen in the lithosphere [e.g. *Silver and Chan*, 1988; *Vauchez and Nicolas*, 1991; *Bastow et al.*, 2007], or combinations of these factors. Seismic phases such as SKS, PKS and SKKS are ideally suited for shear wave splitting studies of the upper mantle beneath a seismograph station because they involve P-to-S conversions at the core-mantle boundary. No source-side anisotropy is preserved, and these phases are horizontally polarized on exiting the core-mantle boundary [e.g. *Savage*, 1999]. Near-vertical incidence of the arrivals also results in good lateral resolution.

1.1. Tectonic History

Our study area in eastern Canada samples over 3 billion years of Earth history, from the core of an Archean craton to the coastal edges of a Paleozoic foldbelt (Figure 1). In the northwest, the regional geology is dominated by the Superior craton, the largest Archean craton on Earth. In this part of the Superior, tectonic subprovinces are largely orientated EW, and comprise fragments of both continental and oceanic affinity [e.g. *Ludden and Hynes*, 2000; *Percival*, 2007]. The Superior craton is bounded to the east and west by Paleoproterozoic orogenic belts, the New Quebec Orogen and Trans-Hudson Orogen, respectively [e.g. *Hoffman*, 1988].

The southeast margin of the craton was affected by several periods of accretion and orogenesis, culminating at ∼1 Ga with the Grenville orogeny, a Himalayan-scale collision associated with the formation of the supercontinent Rodinia [e.g. *Whitmeyer and Karlstrom*, 2007]. The Grenville province and its boundary with the Superior is complex, with a mix of reworked Archean rocks and younger arc material evident in the surface geology. Crustal-scale seismic studies [e.g. *Ludden and Hynes*, 2000] suggest that a significant part of the Grenville crust is underlain by Archean material, though the extent of the Archean lithospheric mantle beneath the present-day Grenville belt remains unclear.

The Rodinia supercontinent began to break up in the late Proterozoic. At this time, there is also evidence for a network of failed rift arms in eastern Canada, such as the Ottawa-Bonnechere graben, which developed prior to the opening of the Iapetus ocean [*Kamo et al.*, 1995]. The southeasternmost part of our study region comprises the Appalachian orogenic belts which resulted from the closure of the Iapetus ocean and accretion of numerous continental fragments in the 462–265 Ma time period [e.g. *Hatcher*, 2005; *van Staal*, 2005]. The culmination of the collisions marked the assembly of the Pangea supercontinent, which subsequently rifted at ∼180 Ma to form the central North Atlantic ocean.

1.2. Previous Geophysical Studies

Seismic anisotropy beneath eastern North America has been studied through measurements of SKS splitting for over 20 years [e.g. *Vinnik et al.*, 1992; *Barruol et al.*, 1997a; *Fouch et al.*, 2000; *Eaton et al.*, 2004; *Frederiksen et al.*, 2007]. A lack of seismograph stations throughout much of Quebec and the Atlantic provinces of Canada has left a large gap in coverage up to recent times; in contrast the eastern US and much of Ontario have been extensively studied. Across the region, the fast-polarisation orientations of SKS splitting are dominated by an ENE—WSW to WNW—ESE trend, as shown from initial sets of measurements at widely-spaced seismograph stations [e.g. *Silver and Chan*, 1991; *Vinnik et al.*, 1992; *Barruol et al.*, 1997a]. With the deployment of closely-spaced networks and arrays, particularly in eastern Canada, smaller-scale variations became apparent. Transects such as Lithoprobe's Abi-94 and Abi-96 [*Sénéchal et al.*, 1996; *Rondenay et al.*, 2000a] provided a dense coverage of data in a NS line straddling the Grenville Front. Along the transect, the EW average fast orientation of the SKS splits rotated progressively from ENE in the north to ESE in the south. More recently, the deployment of the POLARIS network [*Eaton et al.*, 2005] afforded a detailed study of anisotropy in southern and eastern Ontario [e.g. *Eaton et al.*, 2004; *Frederiksen et al.*, 2006, 2007]. In this region, complex sublithospheric flow due to a 'divot' in the cratonic keel [*Fouch et al.*, 2000] was interpreted to play an important role in variations in SKS splitting parameters. Some lithospheric contribution was also inferred; in particular due to correlation between fast-axis changes over a small length-scale with tectonic features such as a failed rift arm [*Eaton et al.*, 2004; *Frederiksen et al.*, 2006]. Detailed studies made at long-term seismograph stations in New England [*Levin et al.*, 1999, 2000a, b] showed significant variation of splitting parameters with earthquake back-azimuth, leading to the interpretation of two distinct anisotropic layers beneath this region. *Bokelmann and Wüstefeld* [2009] compared splitting orientations along the Abi-96 transect to trends in magnetic anomaly patterns. Though the correlations were variable, particularly around the Grenville Front region, they provided support for a significant contribution to the seismic anisotropy from "fossil" fabric related to vertically-coherent lithospheric deformation from past tectonic events.

In addition to measurements from shear-wave splitting alone, seismic anisotropy has been studied beneath continental North America by *Yuan and Romanowicz* [2010] using a combination of splitting measurements with full-waveform analysis. The results present compelling evidence for significant lithospheric anisotropy across the continent, including multiple layers beneath the stable interior. Similar evidence exists from regional-scale surface wave studies in central and northern Canada [e.g. *Darbyshire and Lebedev*, 2009; *Darbyshire et al.*, 2013], as well as global tomographic models [e.g. *Debayle and Ricard*, 2013].

In this paper, we present new shear-wave splitting measurements across eastern Canada from both permanent seismograph stations and more recently-installed networks, covering a region that spans Archean, Proterozoic and Phanerozoic lithosphere. Although station spacing is relatively sparse ($\sim 10^2$ km), these new results represent an important step in the study of structure and processes in a region of eastern North America that has until now only been studied in the context of global/continental-scale tomographic models. The fast-polarisation orientations of the seismic anisotropy are initially compared to lithospheric fabrics inferred from surface geological boundaries and potential-field data. In order to investigate the potential contribution to the splitting from present-day mantle flow, we study the horizontal flow directions inferred from a set of global geodynamic models and compare these to the seismic anisotropy data set for eastern Canada.

2. Data Set and Shear Wave Splitting Measurements

Data from 24 broadband seismograph stations in eastern Canada were used in this study. These consist of a group of 12 permanent stations from the Canadian National Seismograph Network (CNSN) and 12 temporary stations installed during the period 2004–2009 and still in operation at present (Table 1). The temporary stations were deployed through the POLARIS (Portable Observatories for Lithospheric Analysis and Research Investigating Seismicity) project [*Eaton et al.*, 2005] and related initiatives. All stations transmit data continuously, in real time, to the Canadian National Data Centre. Eight stations lie within the Archean Superior craton, eight are situated within the Proterozoic Grenville Province, and the rest are located on Appalachian terranes in Maritime Canada (Figure 1).

We selected earthquakes of magnitude ≥6.0 from the global catalogs, with epicentral distances of 88° or more from the centre of the network. This distance criterion is necessary to separate core S phases (SKS and SKKS) from non-radially polarized phases such as S and ScS. Following basic data processing, we filtered the seismograms between 0.04 and 0.3 Hz, using a 2-pole, Butterworth band-pass filter. Where the signal-to-noise ratio was sufficiently high, we analysed core phases SKS, SKKS and/or PKS arrivals (hereafter all termed 'SKS').

SKS splitting measurements were made using the method of *Teanby et al.* [2004], which is based on the approach of *Silver and Chan* [1991]. The horizontal-component seismograms are rotated and one component is time-shifted so as to minimise the second eigenvalue of particle motion in the analysis window, linearizing particle motion. A grid search over plausible values of ϕ and δt is performed to find the best solution. In the method of *Teanby et al.* [2004], individual measurements are made over a set of 100 windows around the SKS arrival, and a cluster analysis is performed to find the most stable splitting parameters ϕ and δt, as well as an error analysis and a measurement of the source polarisation. Our analysis systematically checks for correspondence between event back-azimuth and source polarisation, to avoid spurious results that would be associated with deep-mantle anomalies, such as those related to the post-perovskite phase transition at D" [e.g. *Restivo and Helffrich*, 2006].

SKS-splitting results typically fall into 2 categories. A split wave initially shows energy on the tangential component and an elliptical particle motion. When the seismograms are corrected for the optimum ϕ and δt, the waveforms will match, the tangential component energy is minimized and the particle motion is linearized. An example is given in Figure 2a. If the wave passes through azimuthally-isotropic material, or if its azimuth is orientated parallel or perpendicular to the fast axis of anisotropy, or if multiple layers of anisotropy cancel out, a characteristic "null" result will be observed (e.g. Figure 2b) [e.g. *Barruol and Hoffmann*, 1999]. In this case, there will be no energy on the tangential component prior to correction, and the uncorrected particle motion will be linear.

A single, horizontal, homogeneous layer of anisotropy can be characterized by a single pair of splitting parameters. Systematic variations with earthquake back-azimuth may indicate a more complex structure, such as the presence of two or more anisotropic layers [e.g. *Levin et al.*, 1999]. Individual results were thus plotted against the source polarisation of the incoming phase (which should be approximately the same as the geometrical back-azimuth) to check for complex structure. Where there was no compelling evidence for systematic variation, we used an analysis based on the method of *Restivo and Helffrich* [1999] to stack the splitting results for each station. The stacks are weighted by signal-to-noise ratio.

3. Results

Individual measurements of splitting orientations (Figure 3a) generally cluster relatively tightly around a dominant direction, and nulls mostly fall along or perpendicular to this direction. We examined the back-azimuthal coverage of the good-quality splitting measurements to ascertain whether there was sufficient evidence of systematic variation in (ϕ, δt) parameters to infer the presence of multiple anisotropic layers. In the case of our data set, despite long recording times at many of the stations, the measurements are largely confined to one or two relatively restricted back-azimuthal ranges (Figure 4). The large gaps in azimuthal coverage do not allow for a direct interpretation of multi-layered anisotropic characteristics, therefore we restrict our quantitative analyses to comparisons with the dominant anisotropic directions inferred from the full sets of measurements. A notable exception is station WEMQ in the north of the study region. The back-azimuthal coverage here is slightly better than average, but almost all measurements gave null results.

Given the general consistency in the individual measurements, we stacked the entire ensemble of results for each station; the resulting splitting orientations are shown in Figure 3b. The dominant splitting orientations range from NE–SW to NW–SE within a broadly E–W average. We note significant changes in splitting orientation between individual stations spaced ∼200–300 km apart. Delay times are also highly variable, ranging from ∼0.3 s (A21) to ∼1.4 s (LATQ, YOSQ). The stacks also show a null result for WEMQ. There does not appear to be a systematic large-scale correlation between delay time or splitting orientation and tectonic province; splitting parameters are particularly variable between stations in the Superior craton. Similarly, the behaviour of splitting parameters at stations close to major tectonic boundaries does not show a systematic pattern. At BELQ, the splitting orientation lies at a shallow angle to the strike of the Grenville Front; however CHGQ and SCHQ show boundary-perpendicular angles with respect to the Grenville Front and the New Quebec Orogen boundaries, respectively. The dominant splitting at ICQ is subparallel to the Appalachian Front, whereas the Charlevoix array stations show an E–W fast orientation, ∼30° away from the local strike of the Appalachian Front.

4. Discussion

Seismic anisotropy in the upper mantle is most commonly attributed to large-scale structural alignments or mineral orientations arising from past or present strain and deformation. Olivine, the most abundant mineral in the upper mantle, is highly intrinsically anisotropic. Strain arising from mantle flow can result in the alignment of olivine *a*-axes in the flow direction [e.g. *Zhang and Karato*, 1995; *Bystricky et al.*, 2000; *Tommasi et al.*, 2000], resulting in an anisotropic fabric due to the crystallographic-preferred orientation (CPO) of olivine, assuming a one-dimensional steady-state shear flow [e.g. *Kaminski and Ribe*, 2002]. Laboratory analyses and sampling of mantle xenoliths suggest that the lithospheric mantle is dominated by *a*-type olivine fabric [*Karato et al.*, 2008]. Evidence exists for other fabric types in the asthenosphere and deep upper mantle; however, away from tectonically-active areas such as subduction zones, the anisotropic fabrics likely present would have a similar effect on SKS waves as the *a*-type [*Karato et al.*, 2008].

4.1. Comparison with Previous Studies

Figure 5 shows the stacked splitting results from this study superimposed on those from previous SKS splitting analyses carried out across the region. The splitting parameters are taken from the global SKS splitting database compiled by Geosciences Montpellier [*Wüstefeld et al.*, 2009] and mirrored by IRIS [*Trabant et al.*, 2012]. The majority of the new values presented in this study cover regions not previously measured. In areas where our new results overlap with previous studies, the agreement between splitting measurements is largely very good (e.g. stations BELQ and MATQ). Station WEMQ in the NW of the study area (∼53N,78W) is an obvious exception, exhibiting an extremely small stacked split, since almost all individual measurements at this station were nulls. A previous study using a much smaller data set [*Frederiksen et al.*, 2007] suggested a larger split; however, the large error bars reported for the splitting parameters suggest that a number of null measurements may have been present.

The vast majority of the seismic anisotropy inferred from shear wave splitting studies is generally attributed to the upper mantle. Lower-mantle anisotropy may give rise to source-polarisation anomalies [e.g. *Restivo and Helffrich*, 2006], or to discrepancies in splitting parameters between SKS and SKKS waveforms. These two phases have similar paths in the upper mantle, but can differ by several hundred kilometers in the lower mantle. *Niu and Perez* [2004] found SKS/SKKS discrepancies at a number of Canadian seismograph stations to the north and west of our study area; however station SCHQ in eastern Canada did not exhibit this property. In our data set, there are a few cases of SKS/SKKS discrepancy, but they do not appear systematic across the network, or for individual station results. We therefore interpret our results in the context of upper-mantle anisotropy only.

4.2. Thickness of anisotropic layer(s)

Measurements of SKS splitting have good lateral resolution of seismic anisotropy in the presence of closely-spaced seismograph networks, but poor depth resolution; interpretations are largely based on the assumption that the anisotropy is found in the upper mantle and the crust but this is generally not directly resolvable. Where station spacing is relatively close ($\sim$100 km), Fresnel-zone arguments can be used to infer the likely depth of the anisotropy [e.g. *Alsina and Snieder*, 1995]. Detailed modeling of the depth ranges of anisotropy can only be carried out where a densely-spaced seismograph network records multiple SKS measurements at a good back-azimuthal coverage [e.g. *Liu and Gao*, 2011].

It is, however, possible to estimate the thickness of an anisotropic layer based on the splitting time, the average shear-wave velocity and the average percentage anisotropy inferred for the layer. To illustrate the likely layer thicknesses associated with our splitting measurements, we use an average percentage anisotropy of 4% [*Savage*, 1999] and shear wave velocities of 4.49–4.65 km/s [*Schaeffer and Lebedev*, 2014]. The layer thickness is given by $L \simeq \delta t < V_s > /dV_s$ where $< V_s >$ is the shear-wave velocity and dV_s is the percentage anisotropy [e.g. *Helffrich*, 1995]. Splitting times are highly variable across our study region, ranging from ∼0.35 s to ∼1.5 s. These values would be consistent with anisotropic layer thicknesses from ∼40 km to ∼160 km if a single homogeneous horizontal layer is assumed. Thicker anisotropic layers would be possible if two or more layers of different orientation interact subtractively.

4.3. Lithospheric Versus Sublithospheric Sources

Patterns of seismic anisotropy can develop due to the preferential alignment of minerals in the crust and/or mantle, the preferential alignment of fluid or melt, or some combination thereof [*Blackman and Kendall*, 1997]. Several tectonic/geodynamic processes could lead to such anisotropy, including: (1) asthenospheric flow in the direction of absolute plate motion [e.g. *Bokelmann and Silver*, 2002; *Heintz et al.*, 2003]; (2) mantle flow around deep cratonic keels [e.g. *Assumpção et al.*, 2006]; (3) pre-existing fossil anisotropy frozen in the lithosphere [e.g. *Silver and Chan*, 1991; *Plomerová and Babuska*, 2010; *Bastow et al.*, 2007]. In the following sections, we discuss the implications of our observations for the lithospheric deformation history of the SE Canada region, and for present-day sublithospheric flow.

4.3.1. Evidence for Complex Anisotropy in North America

Surface-wave and full-waveform tomographic studies on a global [e.g. *Debayle et al.*, 2005; *Debayle and Ricard*, 2013] or regional/continental [e.g. *Yuan et al.*, 2011; *Darbyshire et al.*, 2013] scale have provided compelling evidence for stratification of seismic anisotropy beneath the North American continent. The tomographic model of *Yuan et al.* [2011] suggests that, beneath the North American craton, the lithosphere can be divided into two distinct layers, based on fast axes of azimuthal anisotropy. The layering is strongest beneath the Archean cratons (especially the Superior), but layer 2 appears to pinch out to the east, beneath Grenville-aged surface geology. A third, deeper layer was interpreted by *Yuan et al.* [2011] as sublithospheric anisotropy arising from mantle flow, since they noted a broad scale correlation with regional absolute plate motion (APM) in the HS3 reference frame [*Gripp and Gordon*, 2002].

Although the azimuthal coverage of our data set precludes a detailed analysis of possible anisotropic layering, the tomographic models lend significant support to the hypothesis that both lithospheric and sublithospheric anisotropy contribute to the shear wave splitting observed in this study.

4.3.2. Layered mantle anisotropy and apparent SKS isotropy

We note that the apparent isotropic fabric at station WEMQ, dominated by null measurements, is consistent with the existence of two anisotropic layers which, beneath WEMQ, may have cancelled out the depth-averaged anisotropy. A similar interpretation was made for a station in southern Australia, where analysis of P-S converted phases led to a model of two orthogonal anisotropic layers [*Girardin and Farra*, 1998], whereas SKS splitting measurements gave a null result [*Barruol and Hoffmann*, 1999]. Null measurements in continental lithosphere have been observed in several different regions where the most plausible explanation would be an interaction between multiple anisotropic layers with different orientations; recent examples include the results of *Wagner et al.* [2012] in the SE USA and *Bastow et al.* [2015] in NE Brazil.

4.3.3. Relations Between Splitting Orientations and Surface Tectonics

Within the interior of the Superior craton, there appears to be some correlation between splitting orientations and the strike of individual domains and subprovinces, with splitting directions generally lying subparallel to geologic strikes (Figure 5). This trend breaks down close to the craton boundaries however. In the west (∼80–78°) splitting orientations lie at a shallow angle to the Grenville Front, in contrast to the almost 90° angle observed at station CHGQ. The latter is similar to the angle between the (E–W) splitting measurement at SCHQ and the (N–S) strike of the boundary between the Superior craton and the Paleoproterozoic New Quebec orogen. Similar types of alignment, along with abrupt changes in splitting orientations, were also reported further north and west in the Canadian Shield [*Bastow et al.*, 2011; *Snyder et al.*, 2013; *Frederiksen et al.*, 2013], associated with the boundaries between the Superior and Western Churchill cratons which collided during the Paleoproterozoic Trans-Hudson Orogeny (THO).

In the Grenville Province, variations in splitting orientation in previous studies have previously been attributed to lithospheric features, such as the Ottawa-Bonnechere Graben (WNW of stations ALFO and GAC; *Eaton et al.* [2004]; *Frederiksen et al.* [2006]) or to mantle flow variations [*Fouch et al.*, 2000]. Splitting orientations in the Grenville do not show a large variation over distances of 200–300 km, however delay times are more variable; over twice as great at LATQ than at DMCQ, for example (Figures 3, 5). In the latter case, lithospheric anisotropy may have been affected by the development of the Saguenay graben [*Kumarapeli*, 1985]; DMCQ lies at the northernmost tip of this structure. In Maritime Canada (70–60° W, 43–49° N), splitting orientations are largely subparallel to the strike of boundaries within the Appalachian terranes, though those on the south shore of New Brunswick show a stronger correlation with the coast, perhaps associated with rift structures of the adjacent Fundy basin (Figure 5).

A direct comparison between tectonic features and SKS measurements implies an assumption of vertically-coherent deformation between the crust and the mantle lithosphere [e.g. *Silver and Chan*, 1988, 1991]. This may occur whether or not the tectonic boundaries themselves are vertical, since the anisotropy generally records the orientation of the large-scale deformation. Tectonic processes such as continental collision or large-scale terrane accretion likely cause some degree of coherent deformation throughout both the crust and the mantle lithosphere, resulting in a broad region (up to several hundred km) of orogen-parallel anisotropy [e.g. the Trans-Hudson Orogen, *Bastow et al.*, 2011].

4.3.4. Relations Between Splitting Orientations and Potential Fields

Bokelmann and Wüstefeld [2009] carried out an analysis of correlation between shear wave splitting fast orientations and lineaments in magnetic anomalies to explore possible relationships between structural fabrics in the crust and mantle lithosphere. We examine the new splitting orientations with respect to Bouguer gravity and magnetic anomaly data (source: Geological Survey of Canada). The Bouguer gravity data show very few significant linear trends (with the exception of the Grenville Front low and some highs in Atlantic Canada), but the lineaments and trends in the magnetic data are much more well-defined and thus more informative for comparisons with seismic anisotropy (Figure 6).

Magnetic anomalies are often associated with upper-crustal fabric due to considerations of the r^{-3} intensity-distance relationship and of likely Curie depths within the crust. However, in many stable continental regions, the Curie depth may be as deep as the lower crust, and may penetrate into the topmost lithospheric mantle beneath cratons [e.g. *Bokelmann and Wüstefeld*, 2009, and references therein]. Thus large-scale coherent magnetic lineations likely represent structural features penetrating the entire crust, which may in turn be associated with lithospheric-scale boundaries and deformation zones. For example, in the SE USA, [*Wagner et al.*, 2012] studied magnetic features corresponding to major tectonic features and noted correspondence between SKS splitting orientations and such large-scale lineations.

The characteristics of the magnetic anomalies vary significantly with tectonics (Figure 6). Well-defined lineaments are visible within the Superior craton and the Appalachian terranes. In contrast, aside from the large-scale linear trend at the Grenville Front, the structural fabric within much of the Grenville Province shows localized anomalies rather than linear trends. Similar to the comparison with tectonic boundaries, we note that there is a partial correspondence between splitting orientations and the orientations of magnetic fabric in both the Superior and the Appalachian regions; some splits line up well with magnetic lineaments while others deviate by angles of up to $\sim 45°$. A similar degree of correspondence was noted by *Bokelmann and Wüstefeld* [2009] in their analysis of SKS splits in the Abitibi-Grenville region. Many splitting orientations were shown to have a close correspondence with the predominant directions of magnetic lineaments (as measured by a statistical analysis of degree of alignment), though the results were somewhat variable in nature, especially around the Grenville Front. Angular differences between magnetic trends and SKS splitting orientations peaked around 0±10° but nevertheless showed significant spread, just as we observe in our more qualitative treatment.

The lack of coherent magnetic lineaments in many of the parts of the Grenville Province covered by our splitting data set likely reflects the complexity of the regional tectonic history. The Grenville crust is a combination of reworked Archean and more juvenile material, and Lithoprobe studies [e.g. *Hammer et al.*, 2010] indicate that much of the Grenville Province is underlain by Archean crust at depth. The extent of Archean vs. Proterozoic lithospheric mantle beneath the region is still uncertain. Thus, in this region, crustal magnetic anomalies probably do not reflect large-scale lithospheric fabric, whereas those in both the Superior and the Appalachians likely preserve a clearer record of lithospheric fabric and deformation, with coupling between crust and mantle deformation.

4.3.5. The Role of Sublithospheric Flow

In eastern North America, caution must be used when interpreting anisotropy fast axes in the context of sublithospheric mantle flow using correlation with absolute plate motion (APM). In this region, the 'APM' direction changes significantly depending on whether one considers the Pacific hotspot (HS) reference frame [*Gripp and Gordon*, 2002] or the no-net-rotation (NNR) reference frame [*DeMets et al.*, 1990; *Argus et al.*, 2010], as shown by the arrows in Figure 5. In addition, comparison of global upper-mantle anisotropy from surface-wave tomography with plate motions suggests that basal drag from plate-asthenosphere interaction is likely weak beneath the slower-moving plates [*Debayle and Ricard*, 2013]. Plate-motion calculations for North America give speeds of 16–19 mm/y in the NNR reference frame and 24–29 mm/y in the HS reference frame, well below the threshold of 4 cm/y which *Debayle and Ricard* [2013] quote as the speed at which seismic anisotropy and plate motion correlate well at a full-plate scale.

A more instructive comparison can be made by considering horizontal directions of sub-lithospheric flow derived from global geodynamic models [e.g *Forte*, 2000; *Gaboret et al.*, 2003; *Becker et al.*, 2003]. According to the global study of *Conrad et al.* [2007], simple shear in the asthenosphere rotates the olivine LPO towards the infinite strain axis except for regions close to plate boundaries. Beneath the slow-moving plates, this shear accommodates motion between the relatively stationary lithosphere and the underlying mantle flow, rather than being strongly associated with plate-driven basal drag. These studies of mantle flow induced deformation have long suggested that asthenospheric anisotropy contributes to SKS splitting measurements for both continental and oceanic regions worldwide. However, while it is a dominant factor for oceanic measurements, deviations between mantle flow and seismic anisotropy measurements for continental regions again suggest a significant contribution from "fossil" lithospheric anisotropy. Nevertheless, the relative roles of lithospheric and sublithospheric processes have been debated; some authors [e.g. *Silver and Chan*, 1991; *Silver and Kaneshima*, 1993; *Barruol et al.*, 1997b] suggest that "fossil" anisotropy dominates beneath Precambrian regions, whereas others [e.g. *Vinnik et al.*, 1992, 1995] consider sublithospheric flow to be the major factor in seismic anisotropy beneath cratons.

In Figure 7 we compare the splitting orientations with mantle flow predictions [*Forte et al.*, 2015] based on the seismic-geodynamic global tomography model TX2008 [*Simmons et al.*, 2009], using two different radial viscosity profiles, 'V1' [*Mitrovica and Forte*, 2004] and 'V2' [*Forte et al.*, 2010b]. The main difference between the two profiles in the upper mantle is the thickness of the high-viscosity lithospheric layer: ∼100 km for V1 and ∼200 km for V2. In the following, we consider V1 as having 'normal' lithospheric thickness, in the sense of being representative of a globally-averaged thickness, whereas V2 has a 'thick' lithosphere that may be more representative of subcratonic mantle. The flow calculations are carried out globally up to maximum harmonic degree 128, but are presented here on a finer length scale of $2° \times 2°$ for comparison with the splitting measurements. Inferred flow directions vary depending on the viscosity profile used in the calculations, and are smoothly-varying but non-uniform across the region of interest, reflecting the complexities of the mantle buoyancy distribution beneath this region and the role of vertical flow (upwellings and downwellings). In some regions, the spatial scale of variation is similar to that of the splitting parameters, except for regions of dense seismic data coverage. However, the degree of fit between the splitting orientations and modelled flow directions varies from subparallel to subperpendicular (Figure 7); neither of the two flow predictions provides a uniformly good match to the entire range of variability in the splitting orientations.

Although no single radial profile of mantle viscosity (V1 or V2) appears to explain all the splitting measurements across the entire geographic span of the study region, it is important to note that each profile does yield matches to the splitting observations in different sub-regions. The level of fit is quantified in Figure 8b, through maps of angular deviation between flow direction and splitting orientation. We note that in westernmost Quebec the V2 ('thicker' lithosphere) predictions provide a better overall fit. In contrast, in south-central Quebec the V1 ('normal' lithosphere) predictions generally provide a better match. It is also notable that under the NE US, where seismic tomographic interpretations suggest a lithospheric 'divot' due to the passage of the Great Meteor hotspot [e.g *Eaton and Frederiksen*, 2007], the V1-viscosity predictions yield a distinctly better fit to the splitting observations compared to the V2 results (Figures 7 and 8). These correlations reinforce previous studies suggesting that shear wave splitting observations provide potentially important constraints on the effects of lateral variations in lithospheric thickness [e.g *Fouch et al.*, 2000; *Eaton et al.*, 2004]. This variable thickness, equivalent to lateral variations in viscosity, can be modelled in more complex flow simulations that include 3D viscosity heterogeneity [e.g *Moucha et al.*, 2007]. Such simulations [e.g *Forte et al.*, 2010a] may potentially reconcile the splitting measurements with a single mantle flow model. The verification of this hypothesis requires further modeling of the origin and mapping of lateral viscosity variations [e.g. *Glišović et al.*, 2015] and will be the focus of future work.

In Figure 8a we provide a quantitative summary of the angular deviations calculated between the shear-wave splits and the corresponding flow direction. Although the majority of deviations are less than 20°, several show larger deviations, including near-perpendicular orientations locally. We find some of the largest deviations occur in regions where the predicted radial flow dominates over the horizontal flow (e.g. for the V1-viscosity predictions beneath Maritime Canada in model TX2008-V1; see Figure 7). As discussed above, others occur in regions of substantial horizontal flow such that misfits observed with one viscosity profile (e.g. V1 predictions in central Quebec) are improved using the other. The calculations of deviation also highlight the large variability in splitting orientations over small length scales, such as the dense set of measurements along the Abi-96 transect. This variability is also evident in the individual splitting measurements (Figure 3a).

In addition to degrees of match between modelled flow directions and shear-wave splitting measurements, Fresnel-zone arguments suggest that a significant proportion of the anisotropy likely lies in the upper part of the upper mantle [e.g. *Alsina and Snieder*, 1995]. Beneath the Archean and Proterozoic domains, the lithospheric keel is thick: >150 km; closer to ∼200–250 km in many areas [e.g. *Schaeffer and Lebedev*, 2014], and it is reasonable to expect that "frozen" anisotropic fabric exists within the keel, given the complex tectonic history of the region. Nevertheless, the degree of correlation between the mantle flow models and the splitting orientations suggests that sublithospheric flow may play an important role in the present-day regional seismic anisotropy patterns.

5. Conclusions

SKS-splitting measurements were performed at 24 broadband seismograph stations in eastern Canada, covering a region that spans ∼3/4 of Earth's geological history from the Archean to the Phanerozoic. Station-averaged splitting orientations show a broadly E–W pattern across the region as a whole; however variations in both orientation and delay times are significant at lateral scales of ∼100 km. The splitting orientations align approximately with surface tectonic features in some regions, but make a high angle with both geologic boundaries and magnetic anomaly lineaments in others. Similarly, there is no consistent coherence between the splitting orientations and either North American APM or directions of horizontal sublithospheric flow.

The scale of lateral variability suggests that at least part of the anisotropy giving rise to the shear-wave splits must originate in the lithosphere, through "frozen" structural or mineralogical alignments. However, we infer that sublithospheric flow also plays a significant role. We note that the present-day plate motion beneath eastern North America is slow; thus detailed models of mantle flow rather than a simple treatment related to basal drag of the plate are necessary when considering the sources of sublithospheric anisotropy. The relative roles of fossil lithospheric fabric and sublithospheric flow must be considered carefully in this context.

Particular caution is necessary in studies where backazimuthal coverage is limited, leading generally to hypotheses of a single, horizontal, homogeneous layer of anisotropy to explain the shear-wave splitting measurements. These depth-averaged estimates provide an important first-order constraint on upper mantle anisotropy, but further detailed studies, such as those using surface waves, are necessary to resolve the depths and directions of individual anisotropic layers.

A noteworthy outcome of matching the splitting observations to tomography-based predictions of sublithospheric flow is the apparent sensitivity to the thickness of the lithosphere assumed in the flow simulations. This sensitivity shows that shear wave splitting analyses provide important constraints on lateral variations of subcontinental rheology as reflected in the variability of lithospheric thickness.

Acknowledgments. All original seismograms are freely available either through the IRIS Data Management Center or the Canadian National Data Archive via their respective data request tools. A full list of individual splitting measurements is provided in Supplementary Material. Potential field data are available from the Geological Survey of Canada. For mantle flow directions from the global geodynamic models, please contact the authors.

Bastow acknowledges support from the Leverhulme Trust (grant number P45317). Darbyshire and Forte are funded by NSERC through the Discovery Grants and Canada Research Chairs programmes; these programmes also funded summer internships for Hobbs, Calvel and Gonzalez-Monteza. We also acknowledge the IRIS Consortium's summer internship programme (Schow).

James Wookey provided the codes and SAC [*Goldstein and Snoke*, 2005; *Helffrich et al.*, 2013] macros for the splitting measurements. Map figures were created using GMT software [*Wessel and Smith*, 1998].

We thank the Editors and two anonymous reviewers for their helpful comments which improved the content of the manuscript.

References

Alsina, D., and R. Snieder (1995), Small-scale sublithospheric continental mantle deformation: constraints from SKS splitting observations, *Geophys. J. Int.*, *123*, 431–448, doi:10.1111/j.1365-246X.1995.tb06864.x.

Argus, D., R. Gordon, M. Heflin, C. Ma, R. Eanes, P. Willis, W. Peltier, and S. Owen (2010), The angular velocities of the plates and the velocity of Earth's centre from space geodesy, *Geophys. J. Int.*, *180*, 913–960, doi:10.1111/j.1365-246X.2009.04463.x.

Assumpção, M., M. Heintz, A. Vauchez, and M. Silva (2006), Upper mantle anisotropy in SE and central Brazil from SKS splitting: Evidence of asthenospheric flow around a cratonic keel, *Earth Planet. Sci. Lett.*, *250*(1-2), 224–240, doi:10.1016/j.epsl.2006.07.038.

Barruol, G., and R. Hoffmann (1999), Upper mantle anisotropy beneath the Geoscope stations, *J. Geophys. Res.*, *104*, 10,757–10,773, doi:10.1029/1999JB900033.

Barruol, G., P. G. Silver, and A. Vauchez (1997a), Seismic anisotropy in the eastern United States: Deep structure of a complex continental plate, *J. Geophys. Res.*, *102*, 8329–8348, doi:10.1029/96JB03800.

Barruol, G., G. Helffrich, and A. Vauchez (1997b), Shear wave splitting around the northern Atlantic: frozen Pangaean lithospheric anisotropy?, *Tectonophysics*, *279*, 135–148, doi:10.1016/S0040-1951(97)00126-1.

Bastow, I., T. Owens, G. Helffrich, and J. Knapp (2007), Spatial and temporal constraints on sources of seismic anisotropy: Evidence from the Scottish highlands, *Geophys. Res. Lett.*, *34*, L05305, doi:10.1029/2006GL028911.

Bastow, I., D. Thompson, J.-M. Kendall, G. Helffrich, J. Wookey, D. Snyder, D. Eaton, and F. Darbyshire (2011), Precambrian Plate Tectonics: Seismic Evidence from Northern Hudson Bay, *Geology*, *39*, 91–94, doi:10.1130/G31396.1.

Bastow, I. D., J. Julià, A. do Nascimento, R. Fuck, T. Buckthorp, and J. McClellan (2015), Upper mantle anisotropy of the Borborema Province, NE Brazil: Implications for intra-plate deformation and sub-cratonic asthenospheric flow, *Tectonophysics*, *657*, 81–93, doi:10.1016/j.tecto.2015.06.024.

Becker, T. W., J. B. Kellogg, G. Ekström, and R. J. OConnell (2003), Comparison of azimuthal seismic anisotropy from surface waves and finite strain from global mantle-circulation models, *Geophys. J. Int.*, *155*, 696–714, doi:10.1046/j.1365-246X.2003.02085.x.

Blackman, D., and J.-M. Kendall (1997), Sensitivity of teleseismic body waves to mineral texture and melt in the mantle beneath a mid–ocean ridge, *Philos. Trans. R. Soc. London.*, *355*, 217–231, doi:10.1098/rsta.1997.0007.

Bokelmann, G., and P. Silver (2002), Shear stress at the base of shield lithosphere, *Geophys. Res. Lett.*, *29*, doi:10.1029/2002GL015925.

Bokelmann, G. H., and A. Wüstefeld (2009), Comparing crustal and mantle fabric from the North American craton using magnetics and seismic anisotropy, *Earth Planet. Sci. Lett.*, *277*, 355–364, doi:10.1016/j.epsl.2008.10.032.

Bystricky, M., K. Kunze, L. Burlini, and J.-P. Burg (2000), High shear strain of olivine aggregates: Rheological and seismic consequences, *Science*, *290*, 1564–1567, doi:10.1126/science.290.5496.1564.

Clowes, R. (2010), Initiation, development, and benefits of Lithoprobe — shaping the direction of Earth science in Canada and beyond, *Can. J. Earth Sci.*, *47*, 291–314, doi:10.1139/E09-074.

Conrad, C. P., M. D. Behn, and P. G. Silver (2007), Global mantle flow and the development of seismic anisotropy: differences between the oceanic and continental upper mantle, *J. Geophys. Res.*, *112*, doi:10.1029/2006JB004608.

Darbyshire, F., and S. Lebedev (2009), Rayleigh wave phase-velocity heterogeneity and multilayered azimuthal anisotropy of the Superior Craton, Ontario, *Geophys. J. Int.*, *176*, 215–234, doi:10.1111/j.1365-246X.2008.03982.x.

Darbyshire, F. A., D. W. Eaton, and I. D. Bastow (2013), Seismic imaging of the lithosphere beneath Hudson Bay: Episodic growth of the Laurentian mantle keel, *Earth Planet. Sci. Lett.*, *373*, 179–193, doi:10.1016/j.epsl.2013.05.002.

Debayle, E., and Y. Ricard (2013), Seismic observations of large-scale deformation at the bottom of fast-moving plates, *Earth Planet. Sci. Lett.*, *376*, 165–177, doi:10.1016/j.epsl.2013.06.02.

Debayle, E., B. Kennett, and K. Priestley (2005), Global azimuthal seismic anisotropy and the unique plate-motion deformation of Australia, *Nature*, *433*, 509–512, doi:

10.1038/nature03247.

DeMets, C., R. Gordon, D. Argus, and S. Stein (1990), Current plate motions, *Geophys. J. Int.*, *101*, 425–478, doi:10.1111/j.1365-246X.1990.tb06579.x.

Eaton, D., and A. Frederiksen (2007), Seismic evidence for convection-driven motion of the North American plate, *Nature*, *446*, 428–431, doi:10.1038/nature05675.

Eaton, D., A. Frederiksen, and S.-K. Miong (2004), Shear-wave splitting observations in the lower Great Lakes region; evidence for regional anisotropic domains and keel-modified asthenospheric flow, *Geophys. Res. Lett.*, *31*, doi:10.1029/2004GL019438.

Eaton, D., J. Adams, I. Asudeh, G. Atkinson, M. Bostock, J. Cassidy, I. Ferguson, C. Samson, D. Snyder, K. Tiampo, and M. Unsworth (2005), Investigating Canada's lithosphere and earthquake hazards with portable arrays, *EOS Trans. AGU*, *86*, 169, 173.

Forte, A., R. Moucha, N. Simmons, S. Grand, and J. Mitrovica (2010a), Deep-mantle contributions to the surface dynamics of the North American continent, *Tectonophysics*, *481*, 3–15, doi:10.1016/j.tecto.2009.06.010.

Forte, A., N. Simmons, and S. Grand (2015), Constraints on seismic models from other disciplines - Constraints on 3-D seismic models from global geodynamic observables: Implications for the global mantle convective flow, in *Treatise of Geophysics, 2nd Edition*, vol. 1, edited by B. Romanowicz and A. Dziewonski, pp. 853–907, doi:10.1016/B978-0-444-53802-4.00028-2.

Forte, A. M. (2000), Seismic-geodynamic constraints on mantle flow: implications for layered convection, mantle viscosity, and seismic anisotropy in the deep mantle, in *Earth's Deep Interior: Mineral Physics and Tomography From the Atomic to the Global Scale*, *Geophys. Monogr. Ser.*, vol. 117, edited by S.-I. Karato, A. Forte, R. Liebermann,

G. Masters, and L. Stixrude, pp. 3–36, AGU, doi:10.1029/GM117p0003.

Forte, A. M., S. Quéré, R. Moucha, N. A. Simmons, S. P. Grand, J. X. Mitrovica, and D. B. Rowley (2010b), Joint seismic–geodynamic-mineral physical modelling of African geodynamics: A reconciliation of deep-mantle convection with surface geophysical constraints, *Earth Planet. Sci. Lett.*, *295*, 329–341, doi:10.1016/j.epsl.2010.03.017.

Fouch, M. J., K. M. Fischer, E. Parmentier, M. E. Wysession, and T. J. Clarke (2000), Shear wave splitting, continental keels, and patterns of mantle flow, *J. Geophys. Res.*, *105*(B3), 6255–6275, doi:10.1029/1999JB900372.

Frederiksen, A., I. Ferguson, D. Eaton, S.-K. Miong, and E. Gowan (2006), Mantle fabric at multiple scales across an Archean-Proterozoic boundary, Grenville Front, Canada, *Phys. Earth Planet. Inter.*, *158*, 240–263, doi:10.1016/j.pepi.2006.03.025.

Frederiksen, A., S.-K. Miong, F. Darbyshire, D. Eaton, S. Rondenay, and S. Sol (2007), Lithospheric variations across the Superior Province, Ontario, Canada: Evidence from tomography and shear wave splitting, *J. Geophys. Res.*, *112*, doi:10.1029/2006JB004861.

Frederiksen, A., I. Deniset, O. Ola, and D. Toni (2013), Lithospheric fabric variations in central North America: Influence of rifting and Archean tectonic styles, *Geophys. Res. Lett.*, *40*, 4583–4587, doi:10.1002/grl.50879.

Gaboret, C., A. Forte, and J.-P. Montagner (2003), The unique dynamics of the Pacific Hemisphere mantle and its signature on seismic anisotropy, *Earth Planet. Sci. Lett.*, *208*, 219–233, doi:10.1016/S0012-821X(03)00037-2.

Girardin, N., and V. Farra (1998), Azimuthal anisotropy in the upper mantle from observations of P-to-S converted phases: application to southeast Australia, *Geophys. J. Int.*, *133*, 615–629, doi:10.1046/j.1365-246X.1998.00525.x.

Glišović, P., A. M. Forte, and M. W. Ammann (2015), Variations in grain size and viscosity based on vacancy diffusion in minerals, seismic tomography, and geodynamically inferred mantle rheology, *Geophys. Res. Lett.*, *42*(15), 6278–6286, doi: 10.1002/2015GL065142.

Goldstein, P., and A. Snoke (2005), SAC availability for the IRIS community, *DMS Electronic Newsletter*, *7*.

Gripp, A., and R. Gordon (2002), Young tracks of hotspots and current plate velocities, *Geophys. J. Int.*, *150*, 321–361, doi:10.1046/j.1365-246X.2002.01627.x.

Hammer, P. T., R. M. Clowes, F. A. Cook, A. J. van der Velden, and K. Vasudevan (2010), The Lithoprobe trans-continental lithospheric cross sections: imaging the internal structure of the North American continent, *Can. J. Earth Sci.*, *47*, 821–857, doi:10.1139/E10-036.

Hatcher, J., R.D. (2005), Southern and central Appalachians, in *Encyclopedia of Geology*, edited by R. Selley, L. Cocks, and I. Plinner, pp. 72–81, Elsevier Academic Press, Amsterdam.

Heintz, M., A. Vauchez, M. Assumpção, G. Barruol, and M. Egydio-Silva (2003), Shear wave splitting in SE Brazil: an effect of active or fossil upper mantle flow, or both?, *Earth Planet. Sci. Lett.*, *211*, 79–95, doi:10.1016/S0012-821X(03)00163-8.

Helffrich, G. (1995), Lithospheric deformation inferred from teleseismic shear wave splitting observations in the United Kingdom, *J. Geophys. Res.*, *100*, 18,195–18,204, doi: 10.1029/95JB01572.

Helffrich, G., J. Wookey, and I. Bastow (2013), *The Seismic Analysis Code: A Primer and User's Guide*, Cambridge University Press.

Hoffman, P. (1988), United plates of America, the birth of a craton: Early Proterozoic assembly and growth of Laurentia, *Annu. Rev. Earth Planet. Sci.*, *16*, 543–603, doi: 10.1146/annurev.ea.16.050188.002551.

Kaminski, É., and N. M. Ribe (2002), Timescales for the evolution of seismic anisotropy in mantle flow, *Geochem. Geophys. Geosyst.*, *3*, 1–17, doi:10.1029/2001GC000222.

Kamo, S., T. Krogh, and P. Kumarapeli (1995), Age of the Grenville dyke swarm, Ontario-Quebec: implication for the timing of Iapetan rifting, *Can. J. Earth Sci.*, *32*, 273–280, doi:10.1139/e95-022.

Karato, S.-I., H. Jung, I. Katayama, and P. Skemer (2008), Geodynamic significance of seismic anisotropy of the upper mantle: new insights from laboratory studies, *Annu. Rev. Earth Planet. Sci.*, *36*, 59–95, doi:10.1146/annurev.earth.36.031207.124120.

Kumarapeli, P. (1985), Vestiges of Iapetan rifting in the craton west of the northern Appalachians, *Geoscience Canada*, *12*, 54–59.

Levin, V., W. Menke, and J. Park (1999), Shear wave splitting in the Appalachians and the Urals: a case for multilayered anisotropy, *J. Geophys. Res.*, *104*, 17,975–17,993, doi:10.1029/1999JB900168.

Levin, V., J. Park, M. Brandon, and W. Menke (2000a), Thinning of the upper mantle during late Paleozoic Appalachian orogenesis, *Geology*, *28*, 239–242, doi:10.1130/0091-7613.

Levin, V., W. Menke, and J. Park (2000b), No regional anisotropic domains in the northeastern US Appalachians, *J. Geophys. Res.*, *105*(B8), 19,029–19,042, doi: 10.1029/2000JB900123.

Liu, K. H., and S. S. Gao (2011), Estimation of the depth of anisotropy using spatial coherency of shear-wave splitting parameters, *Bull. Seismol. Soc. Am.*, *101*, 2153–2161, doi:10.1785/0120100258.

Ludden, J., and A. Hynes (2000), The Lithoprobe Abitibi-Grenville transect: two billion years of crust formation and recycling in the Precambrian Shield of Canada, *Can. J. Earth Sci.*, *37*, 459–476, doi:10.1139/e99-120.

Mitrovica, J., and A. Forte (2004), A new inference of mantle viscosity based upon joint inversion of convection and glacial isostatic adjustment data, *Earth Planet. Sci. Lett.*, *225*, 177–189, doi:10.1016/j.epsl.2004.06.005.

Moucha, R., A. Forte, J. Mitrovica, and A. Daradich (2007), Lateral variations in mantle rheology: implications for convection related surface observables and inferred viscosity models, *Geophys. J. Int.*, *169*, 113–135, doi:10.1111/j.1365-246X.2006.03225.x.

Niu, F., and A. M. Perez (2004), Seismic anisotropy in the lower mantle: a comparison of waveform splitting of SKS and SKKS, *Geophys. Res. Lett.*, *31*, doi: 10.1029/2004GL021196.

Percival, J. (2007), Geology and metallogeny of the Superior Province, Canada, in *Mineral deposits of Canada: A synthesis of major deposit-types, district metallogeny, the evolution of geological provinces and exploration methods, Geol. Assoc. Can., Mineral Deposits Division, Spec. Pub.*, vol. 5, edited by W. Goodfellow, pp. 903–928.

Plomerová, J., and V. Babuska (2010), Long memory of mantle lithosphere fabric–European LAB constrained from seismic anisotropy, *Lithos*, doi: 10.1016/j.lithos.2010.01.008.

Restivo, A., and G. Helffrich (1999), Teleseismic shear wave splitting measurements in noisy environments, *Geophys. J. Int.*, *137*, 821–830, doi:10.1046/j.1365-246x.1999.00845.x.

Restivo, A., and G. Helffrich (2006), Core–mantle boundary structure investigated using SKS and SKKS polarization anomalies, *Geophys. J. Int.*, *165*, 288–302, doi:10.1111/j.1365-246X.2006.02901.x.

Rondenay, S., M. Bostock, T. Hearn, D. White, and R. Ellis (2000a), Lithospheric assembly and modification of the SE Canadian Shield: Abitibi-Grenville teleseismic experiment, *J. Geophys. Res.*, *105*, 13,735–13,755, doi:10.1029/2000JB900022.

Savage, M. (1999), Seismic anisotropy and mantle deformation: what have we learned from shear wave splitting, *Rev. Geophys.*, *37*, 65–106, doi:10.1029/98RG02075.

Schaeffer, A., and S. Lebedev (2014), Imaging the North American continent using waveform inversion of global and USArray data, *Earth Planet. Sci. Lett.*, doi:10.1016/j.epsl.2014.05.014.

Sénéchal, G., S. Rondenay, M. Mareschal, J. Guilbert, and G. Poupinet (1996), Seismic and electrical anisotropies in the lithosphere across the Grenville Front, Canada, *Geophys. Res. Lett.*, *23*, 2255–2258, doi:10.1029/96GL01410.

Silver, P. (1996), Seismic anisotropy beneath the continents: Probing the depths of geology, *Annu. Rev. Earth Planet. Sci.*, *24*, 385–432, doi:10.1146/annurev.earth.24.1.385.

Silver, P., and W. Chan (1988), Implications for continental structure and evolution from seismic anisotropy, *Nature*, *335*, 34–39, doi:10.1038/335034a0.

Silver, P., and S. Kaneshima (1993), Constraints on mantle anisotropy beneath Precambrian North America from a transportable teleseismic experiment, *Geophys. Res. Lett.*, *20*, 1127–1130, doi:10.1029/93GL00775.

Silver, P. G., and W. W. Chan (1991), Shear wave splitting and subcontinental mantle deformation, *J. Geophys. Res.*, *96*, 16,429–16,454, doi:10.1029/91JB00899.

Simmons, N. A., A. M. Forte, and S. P. Grand (2009), Joint seismic, geodynamic and mineral physical constraints on three-dimensional mantle heterogeneity: implications for the relative importance of thermal versus compositional heterogeneity, *Geophys. J. Int.*, *177*, 1284–1304, doi:10.1111/j.1365-246X.2009.04133.x.

Sleep, N., C. Ebinger, and J.-M. Kendall (2002), Deflection of mantle plume material by cratonic keels, *Geol. Soc. London. Spec. Pub.*, *199*, 135–150, doi: 10.1144/GSL.SP.2002.199.01.08.

Snyder, D., R. Berman, J.-M. Kendall, and M. Sanborn-Barrie (2013), Seismic anisotropy and mantle structure of the Rae craton, central Canada, from joint interpretation of SKS splitting and receiver functions, *Precambrian Res.*, *232*, 189–208, doi: 10.1016/j.precamres.2012.03.003.

Teanby, N., J.-M. Kendall, and M. Van der Baan (2004), Automation of shear-wave splitting measurements using cluster analysis, *Bull. Seismol. Soc. Am.*, *94*, 453–463, doi:10.1785/0120030123.

Tommasi, A., D. Mainprice, G. Canova, and Y. Chastel (2000), Viscoplastic self-consistent and equilibrium-based modeling of olivine lattice preferred orientations: Implications for the upper mantle seismic anisotropy, *J. Geophys. Res.*, *105*, 7893–7908, doi: 10.1029/1999JB900411.

Trabant, C., A. R. Hutko, M. Bahavar, R. Karstens, T. Ahern, and R. Aster (2012), Data products at the IRIS DMC: Stepping stones for research and other applications, *Seism.*

Res. Lett., *83*(5), 846–854, doi:10.1785/0220120032.

van Staal, C. (2005), Northern Appalachians, in *Encyclopedia of Geology*, edited by R. Selley, L. Cocks, and I. Plinner, pp. 72–81, Elsevier Academic Press, Amsterdam.

Vauchez, A., and A. Nicolas (1991), Mountain building: strike-parallel motion and mantle anisotropy, *Tectonophysics*, *185*, 183–201, doi:10.1016/0040-1951(91)90443-V.

Vinnik, L., V. Farra, and B. Romanowicz (1989), Azimuthal anisotropy in the Earth from observations of SKS at Geoscope and NARS broadband stations, *Bull. Seismol. Soc. Am.*, *79*, 1542–1558.

Vinnik, L., L. Makeyeva, A. Milev, and A. Y. Usenko (1992), Global patterns of azimuthal anisotropy and deformations in the continental mantle, *Geophys. J. Int.*, *111*, 433–447, doi:10.1111/j.1365-246X.1992.tb02102.x.

Vinnik, L., R. Green, and L. Nicolaysen (1995), Recent deformations of the deep continental root beneath southern Africa, *Nature*, *375*, 50–52, doi:10.1038/375050a0.

Wagner, L. S., M. D. Long, M. D. Johnston, and M. H. Benoit (2012), Lithospheric and asthenospheric contributions to shear-wave splitting observations in the southeastern United States, *Earth Planet. Sci. Lett.*, *341–344*, 128–138, doi: 10.1016/j.epsl.2012.06.020.

Wessel, P., and W. Smith (1998), New, improved version of Generic Mapping Tools released, *EOS Trans. AGU*, *79*, 579–579.

Whitmeyer, S., and K. Karlstrom (2007), Tectonic model for the Proterozoic growth of North America, *Geosphere*, *3*, 220–259, doi:10.1130/GES00055.1.

Wüstefeld, A., G. Bokelmann, G. Barruol, and J.-P. Montagner (2009), Identifying global seismic anisotropy patterns by correlating shear-wave splitting and surface-wave data, *Phys. Earth Planet. Inter.*, *176*(3), 198–212, doi:10.1016/j.pepi.2009.05.006.

Yuan, H., and B. Romanowicz (2010), Lithospheric layering in the North American craton, *Nature*, *466*, 1063–1069, doi:10.1038/nature09332.

Yuan, H., B. Romanowicz, K. Fischer, and D. Abt (2011), 3-D shear wave radially and azimuthally anisotropic velocity model of the North American upper mantle, *Geophys. J. Int.*, *184*, 1237–1260, doi:10.1111/j.1365-246X.2010.040901.x.

Zhang, S., and S.-I. Karato (1995), Lattice preferred orientation of olivine aggregates deformed in simple shear, *Nature*, *375*, 774–777, doi:10.1038/375774a0.

Figure 1. (a) Tectonic map of eastern Canada [after *Clowes*, 2010] and seismograph stations (inverted triangles) used in this study. The pentagon represents 6 stations of the Charlevoix Array (CA): A11, A16, A21, A54, A64 and LMQ. Regions as follows: ON - Ontario, QC - Québec, NB - New Brunswick, NL - Newfoundland and Labrador, NS - Nova Scotia, ME - Maine (USA). (b) Earthquakes (circles) used in SKS splitting measurements; the map is centred on our study region (star).

Figure 2. Examples of shear-wave splitting analysis. (a) A high-quality split. (i) original 3-component seismogram (east, north, vertical) showing the SKS phase and subsequent arrivals, along with the chosen analysis window (marked START, END), (ii) radial and tangential components before (top) and after (bottom) correction by the splitting analysis; tangential SKS energy is minimized, (iii) windowed waveforms (dashed line: fast, solid line: slow) before and after correction; plot 2 is normalized and plot 3 shows the corrected waves with their relative amplitudes preserved, (iv) particle motion before and after correction, showing the change from elliptical to linearized motion, (v) grid-search and cluster analysis outputs. The main graphic shows the final grid search results for ϕ and δt; the two smaller plots show individual measurements of ϕ and δt for the 100 windows used in the analysis. (b) A high-quality null. In this case, there is no signal on the tangential-component waveform, and the particle motion is linear both before and after analysis.

Figure 3. (a) Compilation of individual high-quality splitting measurements for the eastern Canadian stations. Blue bars show splits and black crosses indicate nulls (showing the 90° ambiguity). (b) Results of stacking the individual measurements at each station. Ticked lines AF and GF show the Appalachian and Grenville fronts, respectively. CA: Charlevoix array (stations A11, A16, A21, A54, A64, LMQ).

Figure 4. Examples of the back-azimuthal coverage of good-quality splitting results for 4 representative stations: NEMQ/NMSQ (Superior), LATQ and A54 (Grenville), and GGN (Appalachians). Similar coverage is seen for the rest of the network. For each station, the top graph shows fast orientations; squares represent null measurements and circles with error bars are splits. The bottom graph shows delay times for the splits only (since δt is undefined for nulls).

Figure 5. Comparison of the new stacked SKS splits (red bars) with previous measurements (purple bars) taken from the global shear-wave splitting data base [*Wüstefeld et al.*, 2009; *Trabant et al.*, 2012], superimposed on tectonic boundaries [after *Clowes*, 2010]. The two arrows show absolute plate motion (APM) in two different reference frames: Nuvel-NNR (*DeMets et al.* [1990]; green) and HS3 (*Gripp and Gordon* [2002]; black). Ticked lines AF and GF show the Appalachian and Grenville fronts, respectively.

Figure 6. SKS splits (red and purple bars) superimposed on a magnetic anomaly map of Canada (Geological Survey of Canada).

Figure 7. Comparisons between SKS splitting fast orientations and flow-related fabrics from 2 geodynamic models. Red/purple bars: anisotropy measurements from SKS splitting; Blue arrows: horizontal component of instantaneous mantle flow. The same seismic tomography model but different radial viscosity models are used to calculate the flow magnitudes and directions.

Figure 8. (a) Histogram of angular deviation between shear-wave splitting orientations and horizontal mantle flow directions (after correction for the 180° ambiguity inherent in the orientations), for mantle flow models TX2008-V1 and TX2008-V2 [*Simmons et al.*, 2009; *Mitrovica and Forte*, 2004; *Forte et al.*, 2010a]. (b) Maps of angular deviations across eastern Canada for the two different flow models. The black stars in map TX2008-V1 indicate a region where the flow is dominantly radial, precluding a direct comparison with SKS azimuthal anisotropy. The five stations are therefore not included in the V1 histogram in (a). Station WEMQ (null split) is shown as a black square in the maps.

Table 1. List of seismograph stations used in the study[a]

Station Code	Latitude	Longitude	Elev (km)	Network	Operation
A11	47.2425	-70.1978	0.06	CNSN	2000—present
A16	47.4706	-70.0064	0.02	CNSN	2000—present
A21	47.7036	-69.6897	0.05	CNSN	2000—present
A54	47.4567	-70.4125	0.38	CNSN	2000—present
A64	47.8264	-69.8922	0.14	CNSN	2000—present
ALFO	45.6283	-74.8842	0.00	POLARIS	2004—present
BATG	47.2767	-66.0599	0.34	POLARIS	2005—present
BELQ	47.3980	-78.6874	0.36	POLARIS	2007—present
CHGQ	49.9105	-74.3748	0.41	POLARIS	2007—present
DMCQ	48.9646	-72.0680	0.20	POLARIS	2009—present
GAC	45.7033	-75.4783	0.06	CNSN	1992—present
GBN	45.4067	-61.5133	0.04	CNSN	2005—present
GGN	45.1184	-66.8420	0.03	CNSN	2002—present
ICQ	49.5217	-67.2719	0.06	CNSN	2001—present
LATQ	47.3836	-72.7819	0.16	POLARIS	2007—present
LMN	45.8520	-64.8060	0.36	CNSN	1993—present
LMQ	47.5485	-70.3258	0.43	CNSN	1998—present
LSQQ	49.0580	-76.9796	0.31	POLARIS	2009—present
MATQ	49.7589	-77.6376	0.28	POLARIS	2007—present
NEMQ	51.6837	-76.2576	0.20	POLARIS	2007–2009
NMSQ	51.7133	-76.0237	0.28	POLARIS	2009—present
SCHQ	54.8324	-66.8332	0.50	CNSN	1998—present
WEMQ	53.0535	-77.9737	0.17	POLARIS	2005—present
YOSQ	52.8666	-72.1998	0.65	POLARIS	2005—present

[a] Network affiliations as follows - CNSN: Canadian National Seismograph Network, POLARIS: Portable Observatories for Lithospheric Analysis and Research Investigating Seismicity.

Table 2. Stacked SKS splitting parameters for each station[b]

Station Code	Orientation (^{o})	Delay time (s)	Number	Previous measurements
A11	90 ± 1.25	0.90 ± 0.03	16	
A16	-88 ± 1.75	0.83 ± 0.06	9	
A21	-87 ± 3.00	0.33 ± 0.02	13	
A54	-83 ± 1.25	0.80 ± 0.03	14	
A64	-89 ± 1.25	0.63 ± 0.02	22	
ALFO	75 ± 2.50	0.88 ± 0.07	4	
BATG	-86 ± 5.00	0.53 ± 0.03	6	
BELQ	-83 ± 1.00	0.65 ± 0.02	11	
CHGQ	-64 ± 2.75	0.70 ± 0.01	7	
DMCQ	82 ± 6.25	0.60 ± 0.04	3	
GAC	75 ± 2.25	0.48 ± 0.03	12	85^o/0.9s ; 36^o/0.65s ; 61 ± 13^o/0.5 ± 0.3s
GBN	-84 ± 1.50	0.68 ± 0.03	7	
GGN	67 ± 1.00	1.03 ± 0.03	9	
ICQ	82 ± 4.75	0.68 ± 0.06	5	
LATQ	-82 ± 1.00	1.40 ± 0.02	20	
LMN	76 ± 1.75	1.15 ± 0.06	5	78^o/1.3s ; 83^o/1.48s
LMQ	83 ± 2.00	1.03 ± 0.07	7	87^o/1.3s ; 83^o/1.1s
LSQQ	85 ± 2.00	0.73 ± 0.11	3	
MATQ	79 ± 1.00	0.83 ± 0.03	10	
NEMQ	43 ± 1.75	0.63 ± 0.10	4	
NMSQ	50 ± 1.00	0.63 ± 0.10	17	
SCHQ	80 ± 1.00	0.65 ± 0.03	11	
WEMQ	62 ± 7.25	0.13 ± 0.02	18	65 ± 52^o/0.75 ± 0.65s
YOSQ	64 ± 1.75	1.33 ± 0.06	6	

[b] Note that the large errors and small delay-time value at station WEMQ are due to the abundance of null results at this station. Results from the literature, where available, are given in pairs of splitting orientation / delay time. Semicolons separate the results of multiple studies or a single study using multiple methods.

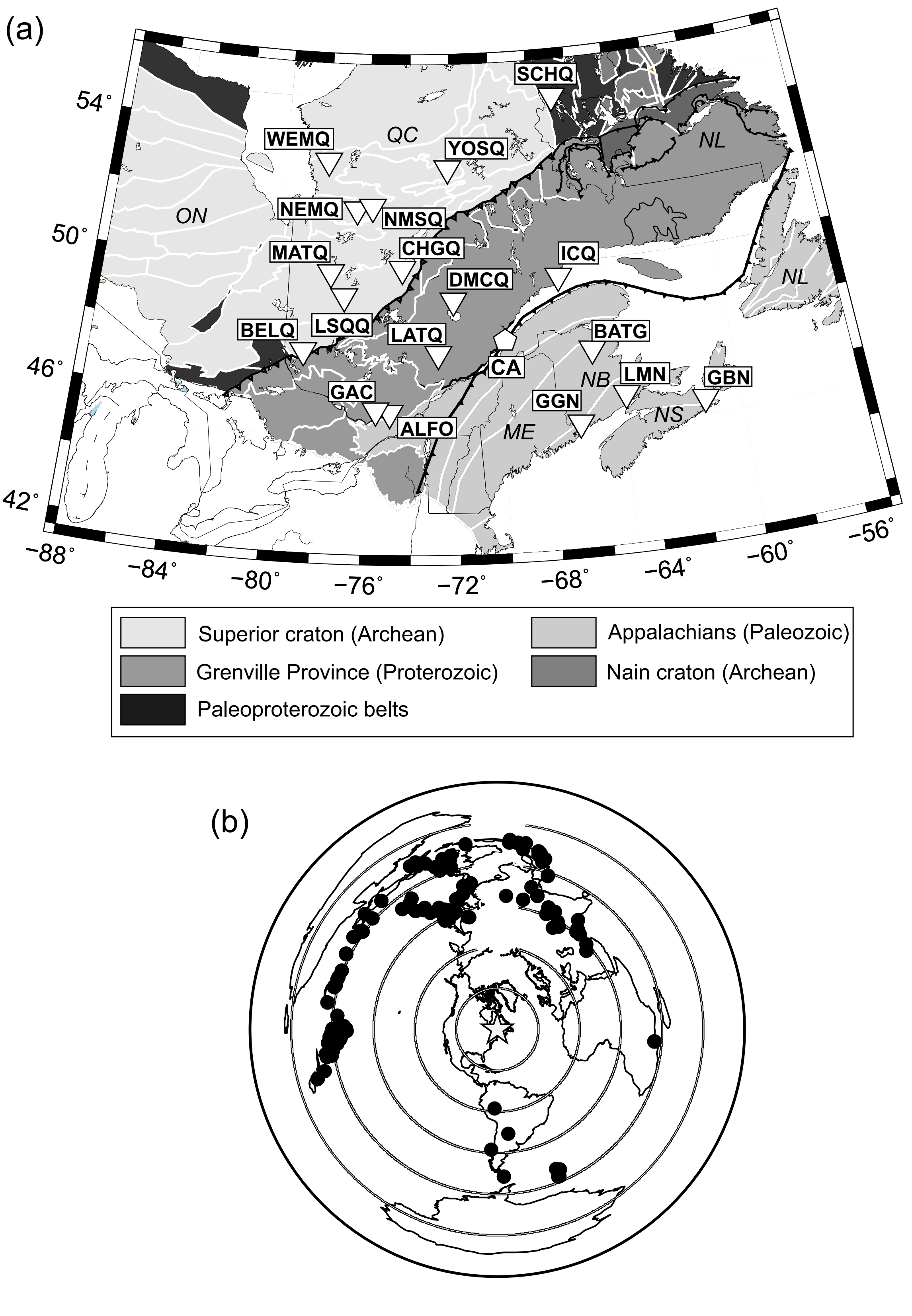

(a)
54°
50°
46°
42°
−88°
−84°
−80°
−76°
−72°
−68°
−64°
−60°
−56°
SCHQ
WEMQ
QC
YOSQ
NL
ON
NEMQ
NMSQ
MATQ
CHGQ
ICQ
DMCQ
NL
BELQ
LSQQ
LATQ
BATG
CA
NB
LMN
GBN
GAC
GGN
NS
ALFO
ME
Superior craton (Archean)
Appalachians (Paleozoic)
Grenville Province (Proterozoic)
Nain craton (Archean)
Paleoproterozoic belts
(b)

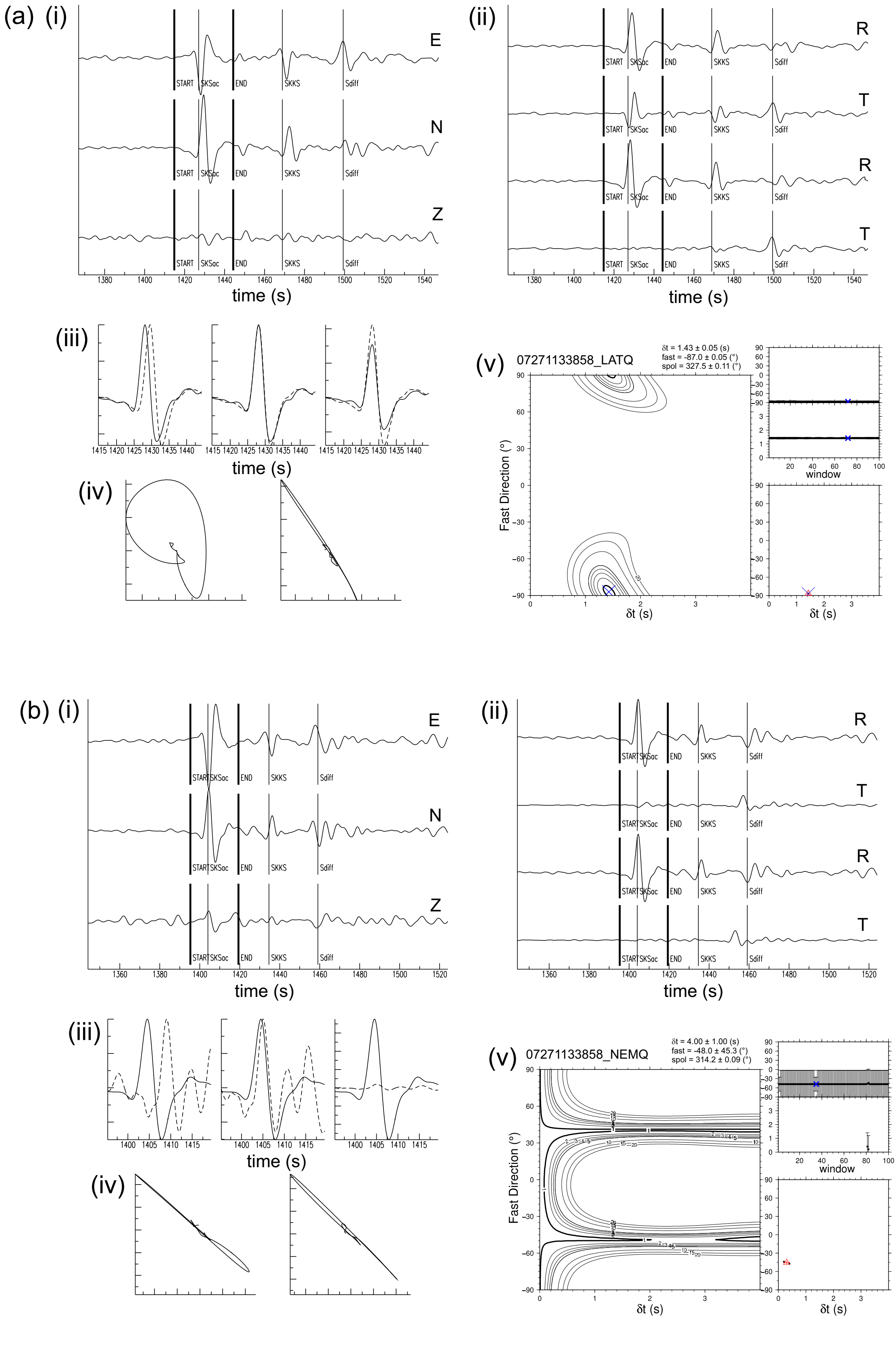
(a) (i)
E
N
Z
START
SKSac
END
SKKS
Sdiff
time (s)
(ii)
R
T
R
T
(iii)
time (s)
(iv)
(v)
07271133858_LATQ
δt = 1.43 ± 0.05 (s)
fast = -87.0 ± 0.05 (°)
spol = 327.5 ± 0.11 (°)
Fast Direction (°)
δt (s)
window
(b) (i)
E
N
Z
time (s)
(ii)
R
T
R
T
time (s)
(iii)
time (s)
(iv)
(v)
07271133858_NEMQ
δt = 4.00 ± 1.00 (s)
fast = -48.0 ± 45.3 (°)
spol = 314.2 ± 0.09 (°)
Fast Direction (°)
δt (s)
window

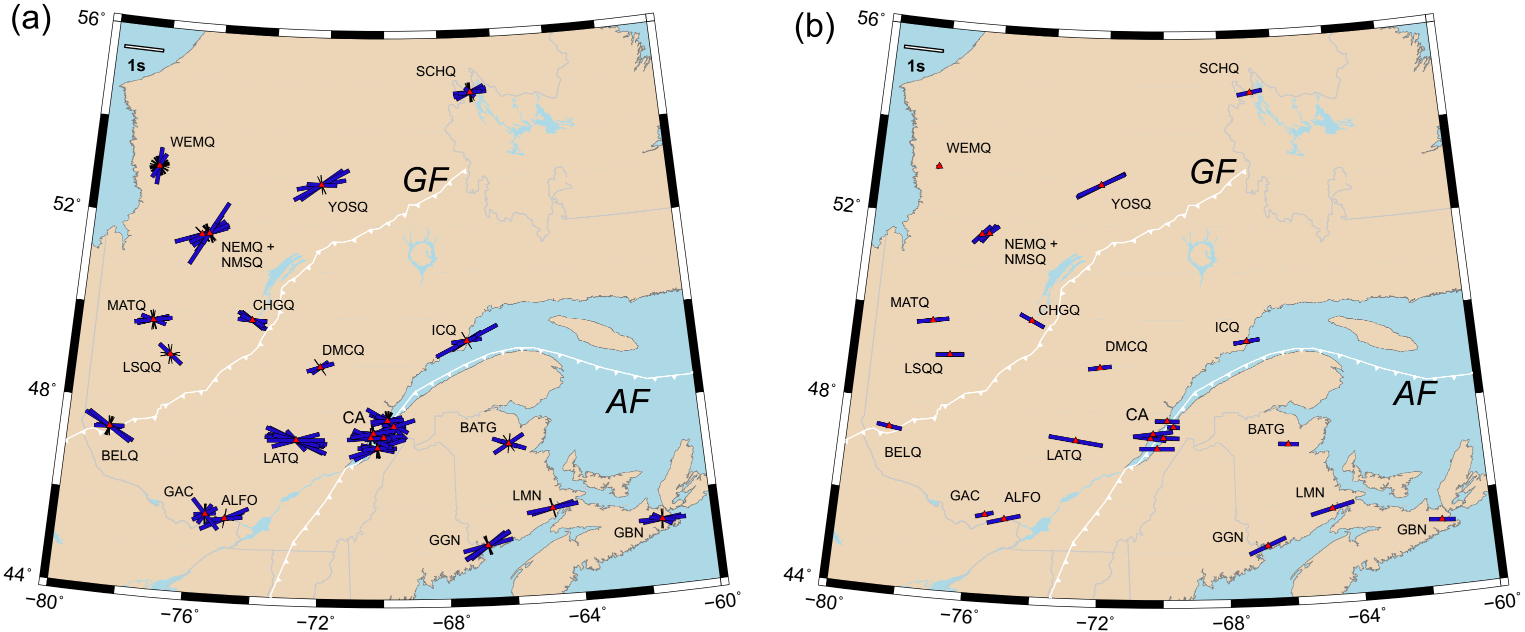

(a)
(b)
1s
56°
52°
48°
44°
-80°
-76°
-72°
-68°
-64°
-60°
GF
AF
SCHQ
WEMQ
YOSQ
NEMQ +
NMSQ
MATQ
CHGQ
LSQQ
DMCQ
ICQ
CA
BELQ
LATQ
BATG
GAC
ALFO
LMN
GGN
GBN

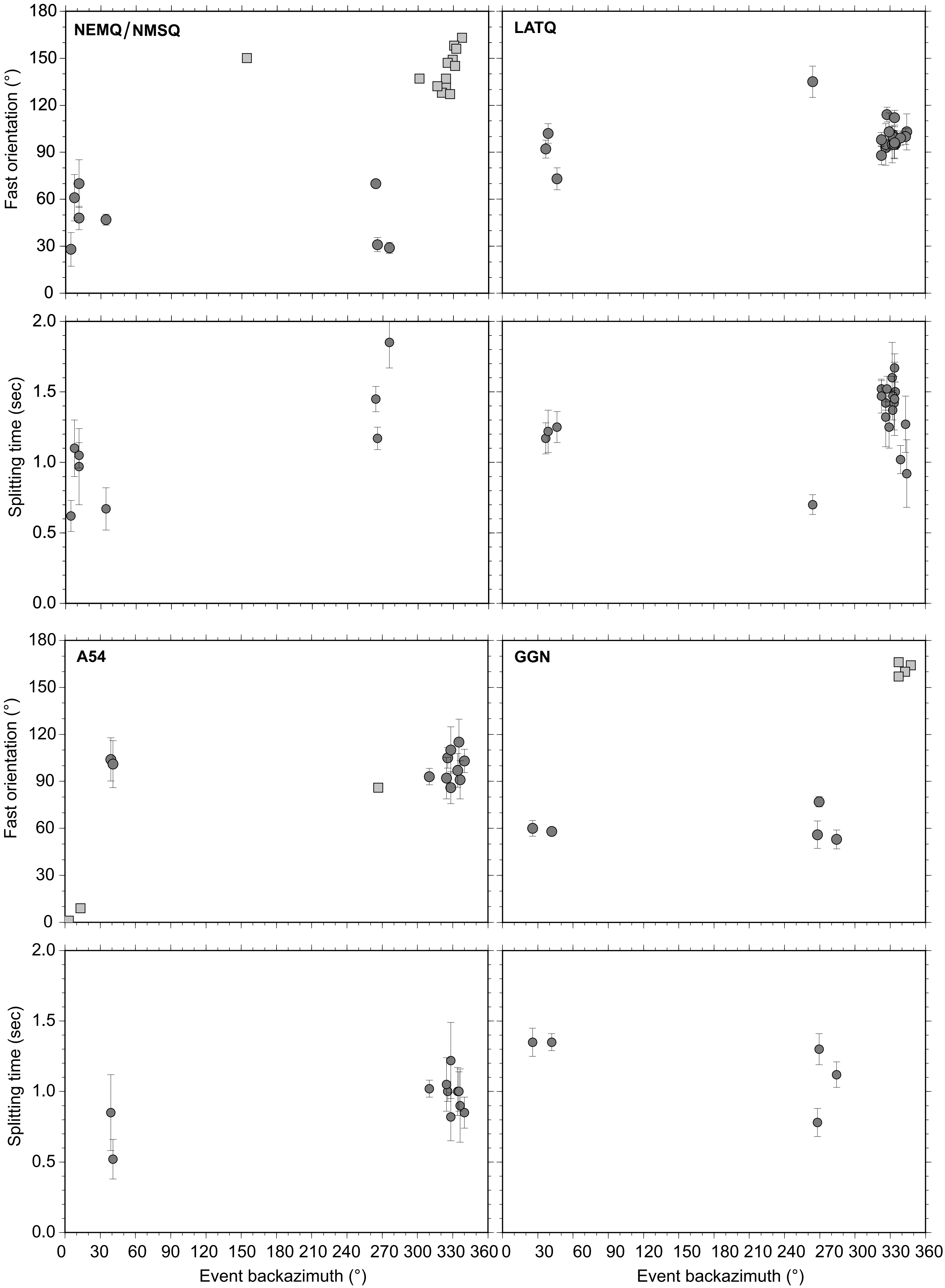
NEMQ/NMSQ
LATQ
A54
GGN
Fast orientation (°)
Splitting time (sec)
Event backazimuth (°)
0
30
60
90
120
150
180
0.0
0.5
1.0
1.5
2.0
0 30 60 90 120 150 180 210 240 270 300 330 360

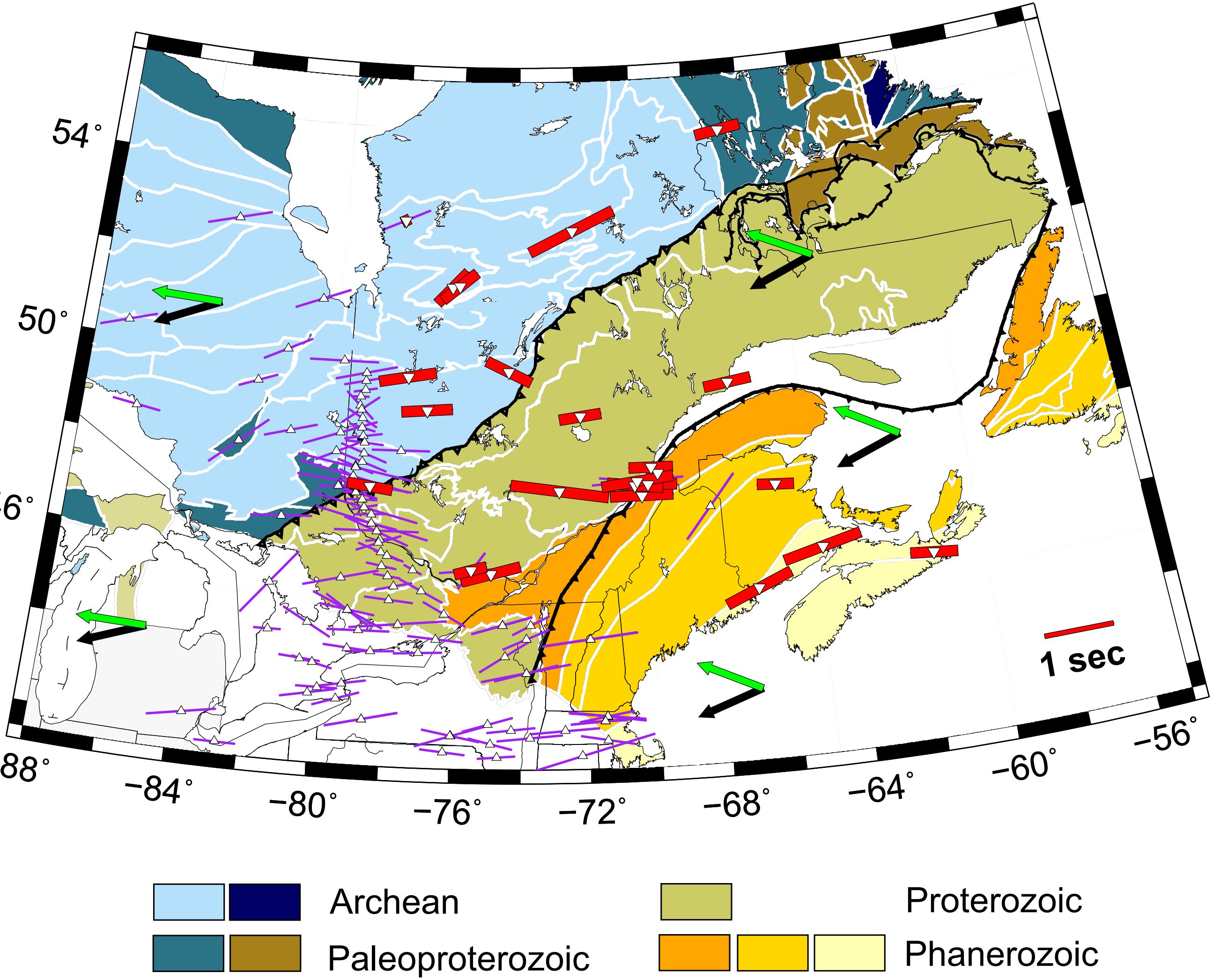

54°
50°
46°
42°
−88°
−84°
−80°
−76°
−72°
−68°
−64°
−60°
−56°
1 sec
Archean
Paleoproterozoic
Proterozoic
Phanerozoic

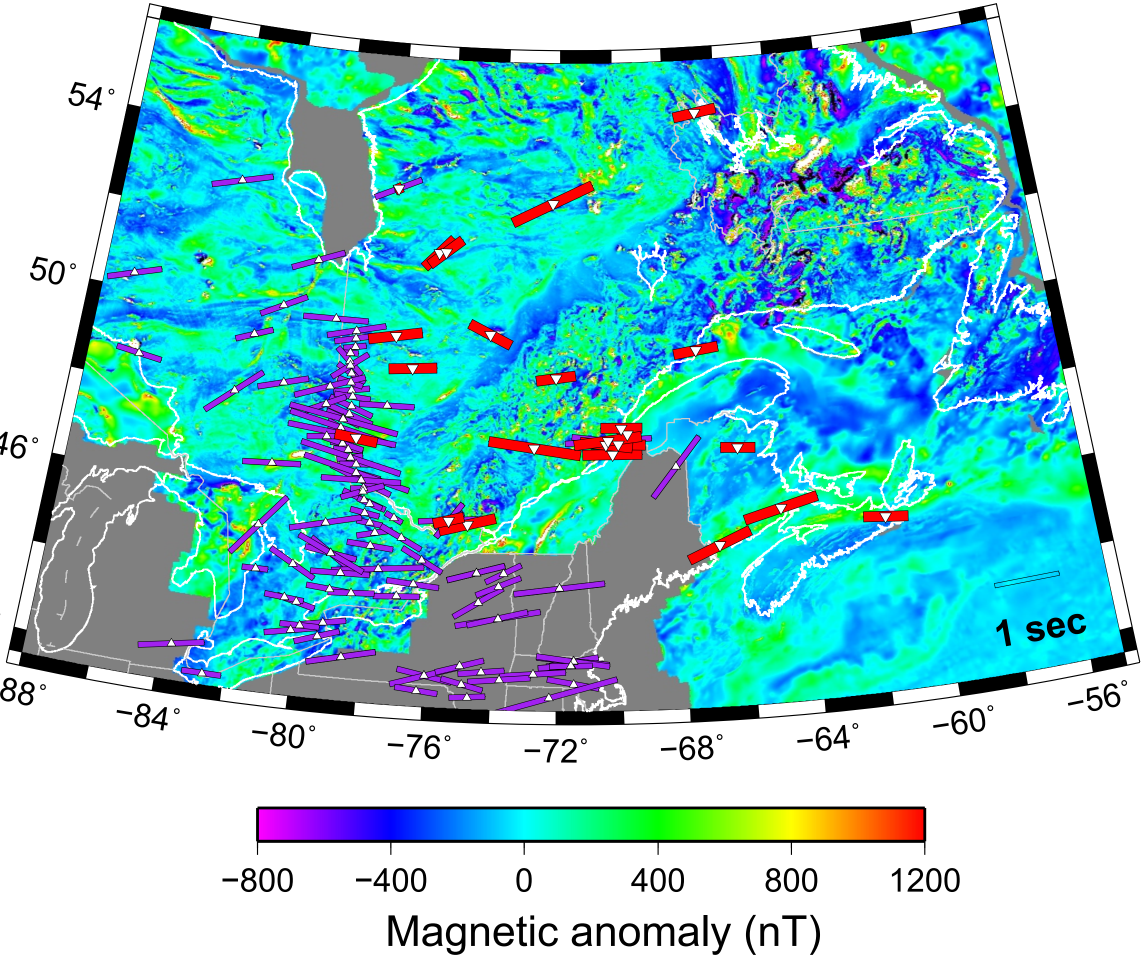
54°
50°
46°
42°
−88°
−84°
−80°
−76°
−72°
−68°
−64°
−60°
−56°
1 sec
−800
−400
0
400
800
1200
Magnetic anomaly (nT)

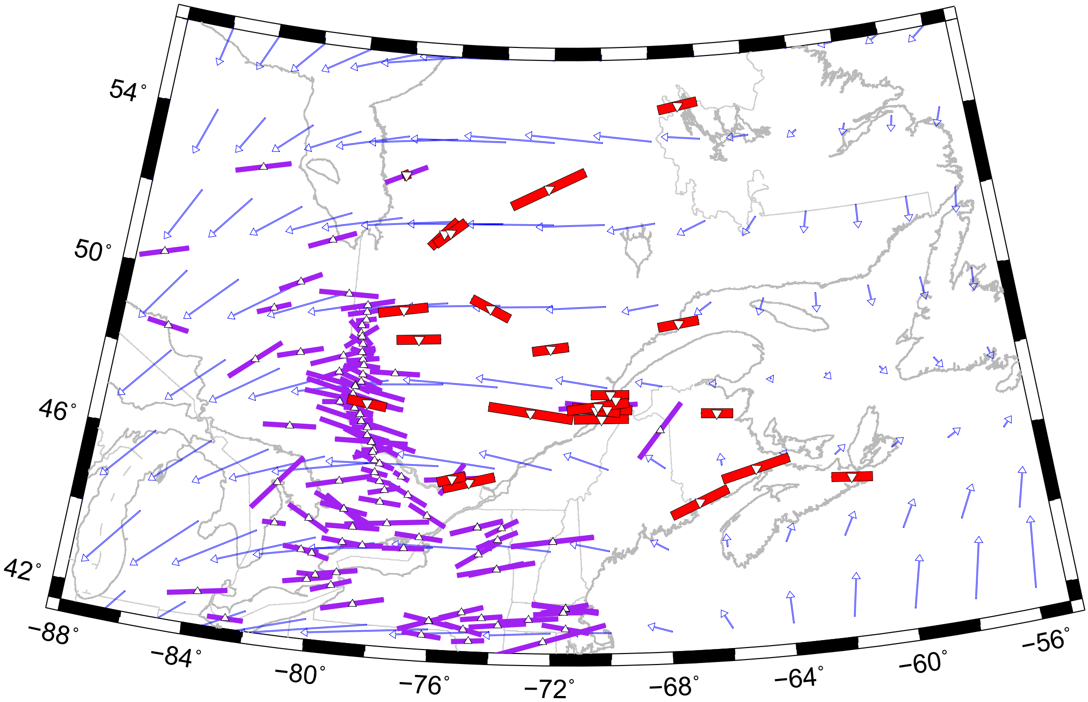

TX2008−V1 2 cm/yr
TX2008−V2 2 cm/yr

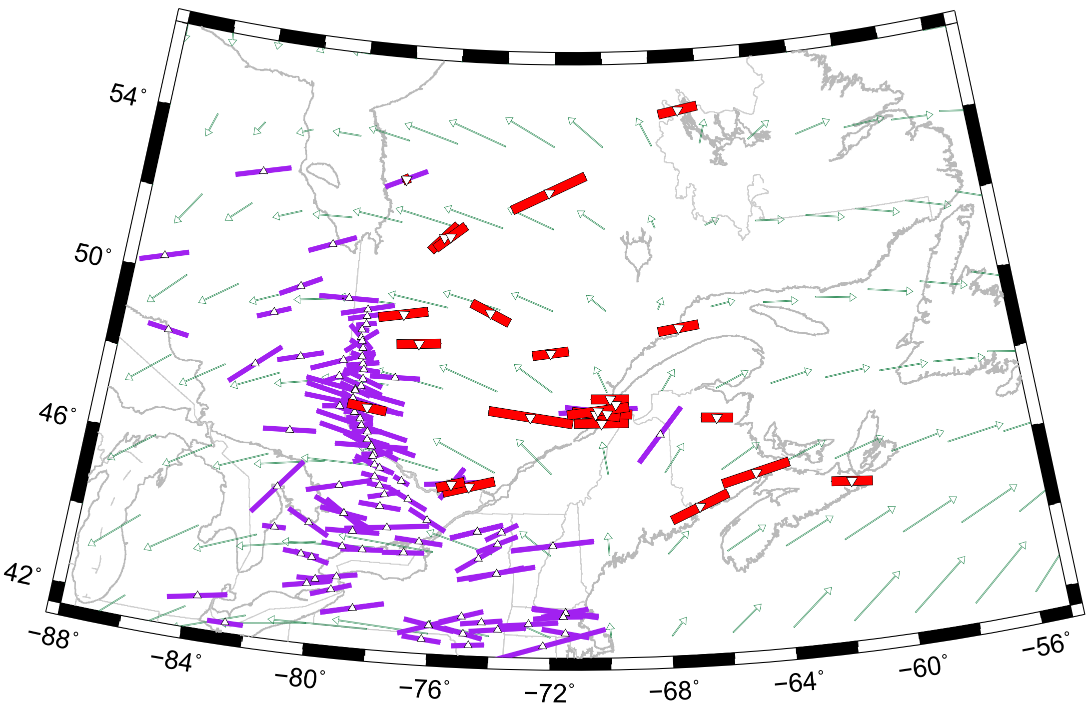

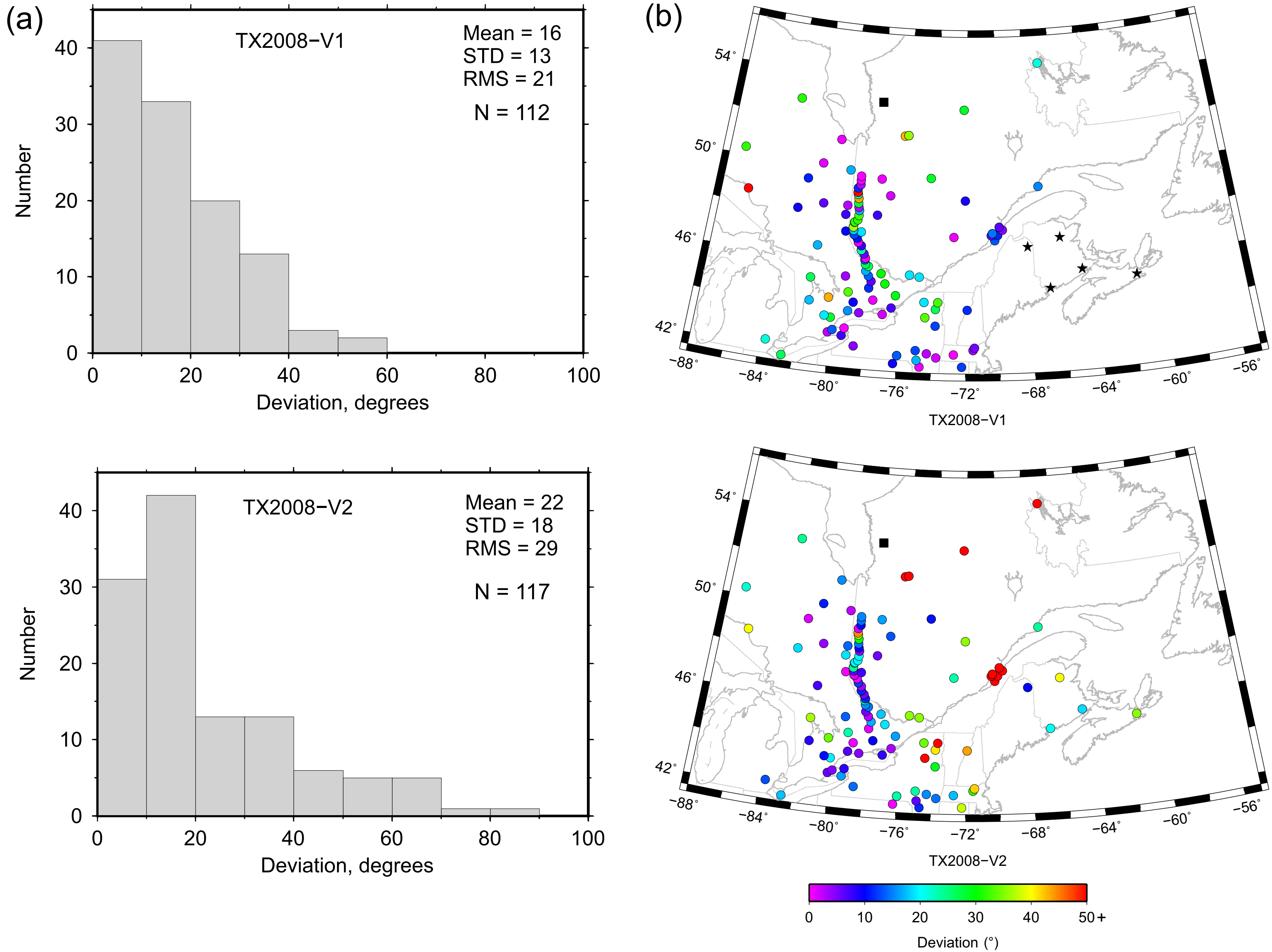
(a)
TX2008−V1
Mean = 16
STD = 13
RMS = 21
N = 112
Number
Deviation, degrees
TX2008−V2
Mean = 22
STD = 18
RMS = 29
N = 117
(b)
TX2008−V1
TX2008−V2
Deviation (°)
50+